

RESEARCH ARTICLE

Gold Nanoparticles Introduced ZnO/Perovskite/Silicon Heterojunction Solar Cell

JASURBEK GULOMOV¹ AND OUSSAMA ACCOUCHE², (Associate Member, IEEE)

¹Renewable Energy Sources Laboratory, Andijan State University, Andijan 170100, Uzbekistan

²College of Engineering and Technology, American University of the Middle East, Egaila 54200, Kuwait


Corresponding author: Jasurbek Gulomov (jasurbekgulomov@yahoo.com)

ABSTRACT Renewable energy sources like photovoltaics have the potential to mitigate the negative consequences of pollution and global warming. The solar sector has shown exponential growth and is quickly becoming a viable alternative to fossil fuels. Currently, the great majority of solar modules are composed of crystalline silicon. To make photovoltaics more competitive, affordability and efficiency are two of the most important elements. Metal nanoparticles can be introduced or a heterojunction can be made using appropriate materials to increase the absorption coefficient of a silicon-based solar cell, which boost the total efficiency of the solar module. Therefore, in this study, we used Sentaurus TCAD simulation to examine the effects of gold nanoparticles introduced with various sizes and periodicities on the photoelectric characteristics of ZnO/Si and Perovskite/Si solar cells. Accordingly, all of the photoelectric characteristics of the perovskite/Si solar cell have shown a clear sinusoidal connection with the nanoparticle periodicity. When the gold nanoparticle size changed from 6 nm to 9 nm, the period of the sinusoidal function changed to π . The photoelectric parameters of ZnO/Si solar cells changed in a sinusoidal pattern based on the nanoparticle's periodicity, but this was true only when the nanoparticles size was between 9 nm and 21 nm. According to the obtained results, the maximum values of short-circuit current, open circuit voltage and fill factor are 10.47 mA/cm², 0.384 V, 71.06% for perovskite/Si and 10.52 mA/cm², 0.306 V, 71.12% for ZnO/Si. The minimum current density of the perovskite/Si solar cell was identical when compared to the solar cell without nanoparticles. When a gold nanoparticle with a size of 6 nm was introduced into the ZnO/Si solar cell with a periodicity of 120 nm, the short circuit current decreased by a factor of 3.81 compared to the solar cell without the nanoparticle. It has been scientifically proven that Fano interference is responsible for the sinusoidal relationship between the short-circuit current of the solar cells and the periodicity of the nanoparticle.

INDEX TERMS Numerical simulation, heterojunctions, nanoparticles, silicon, perovskites.

I. INTRODUCTION

Today, a lot of scientific research is being conducted to increase the efficiency of solar cells and reduce their cost. The industry mainly produces silicon-based solar cells [1]. Although, lots of scientific work has been done to optimize the size [2], surface morphology [3], doping concentration [4] and device structure of silicon-based solar cells, silicon-based solar cells are still considered to have high production cost along with a modest efficiency of 22.8% [5]. In addition, the efficiency of pure silicon-based solar cells cannot exceed the theoretical value of 29% according to the Shockley-Quisser

The associate editor coordinating the review of this manuscript and approving it for publication was Chong Leong Gan .

theory [6]. However, we can increase this upper limit to 42% by forming nanostructures on its surface [7]. Furthermore, it has been discovered that adding platinum metal nanoparticles to the solar cells can double their efficiency [8].

Other materials instead of silicon for solar cells have been extensively researched. For example, despite the high cost of GaAs-based solar cells, it has been determined that they are the most suitable for use in space and have high radiation resistance [9]. In the last 10 years, interest in perovskite structures has increased dramatically [10]. Because perovskite materials have a high absorption coefficient in thin layers [11]. Perovskite materials are also divided into organic and organic-inorganic hybrid types [12]. Among them, the most widely used for making solar cells is CH₃NH₃PbI₃ [13].

The bandgap of $\text{CH}_3\text{NH}_3\text{PbI}_3$ is 1.55 eV [14], approximately equal to that of GaAs. In addition, it is a direct semiconductor like GaAs. Electron transport layer (ETL) and hole transport layers (HTL) are used to optimize perovskite-based solar cells and to better separate charge carriers [15]. ETL and HTL are selected depending on the type of perovskite material, the band gap, the electron density and the crystal lattice constant. In solar cells based on $\text{CH}_3\text{NH}_3\text{PbI}_3$, ZnO [16], SnO_2 [17] as ETL and NiO_x [18], Spir-Ometad [19] as HTL are widely used. By optimizing ETL, HTL, the perovskite layer thicknesses and its input concentration, its efficiency can be increased up to 29.53% [20] and up to 33% according to the Shockley-Quisser theory [21]. Perovskite-based solar cells are divided into two types according to the arrangement of the layers [22]: direct and inverted. Perovskite solar cells are mainly formed by preparing a solution and depositing it on a substrate [23]. The efficiency of the planar $\text{CH}_3\text{NH}_3\text{PbI}_3$ -based inverted solar cell was experimentally reported to be 13.97% when a 1.3:1.3 M mixture of PbI_2 - $\text{CH}_3\text{NH}_3\text{I}$ was produced by spinning at a speed of 4000 rpm [24]. To increase the efficiency of solar cells, surface textures [25], coating with optical layers [26] and introduction of nanoparticles [27] or quantum dots [28] are used in practice.

So far, silicon, simple perovskite and perovskite/silicon tandem solar cells have been well studied [29]. Even the effect of nanoparticles introduced into silicon, perovskite and organic solar cells [30] have been well studied. In our previous research, we studied ZnO/Si and perovskite/Si heterojunction solar cells and determined their optimal thicknesses [31]. However, nanoparticle-incorporated ZnO/Si and perovskite/Si solar cells have hardly been studied. Therefore, in this scientific work, the effect of gold nanoparticles of different sizes and periodicities on ZnO/Si and perovskite/Si solar cells of optimal thicknesses is studied.

II. MATERIALS AND METHODS

A. SIMULATION PROCEDURE

There are 3 main methods used to study solar cells: theory, experiment and simulation. In this scientific work, the simulation method was used for the study of ZnO/Si and Perovskite/Si heterojunctions with gold nanoparticles. There are a lot of simulation tools for solar cells [32]. Sentaurus TCAD software was used for simulation. The Sentaurus Structure Editor tool of the Sentaurus TCAD program was used to create a geometric model of the solar cell. In our earlier research papers, we described in great detail how to use the Sentaurus Structure Editor and the Tool Command Language to create solar cells and nanoparticles of varying structures through the use of a single loop algorithmic. [33].

Each material in a solar cell is given a set of physical properties in Sentaurus Device once its geometric model is created. The material base of Sentaurus TCAD contains almost all the physical parameters of monocrystalline silicon. As we have studied simple planar ZnO/Si and Perovskite/Si solar cells in our previous scientific works, parameter files of perovskite and ZnO have been created and added to the

material base of Sentaurus TCAD. The Sentaurus TCAD material database contains a parameter file for gold, but some of its physical parameters need some modifications according to the size of the nanoparticle. Because in Sentaurus TCAD parameter files are given for bulk materials. When the size of the material is reduced to the nanoscale, some of its physical parameters change due to the size effect [29]. The physical parameters of the gold nanoparticle differ from those of the bulk gold. Because as the size of a nanoparticle decreases, its surface per unit volume increases significantly.

Given the required physical models and mathematical methods for the solar cell, Sentaurus Device is able to perform numerical simulation. Unlike other semiconductor devices, solar cells simulation requires optical properties in addition to the electrical ones. In this scientific work, AM1.5g light spectrum was used to illuminate the solar cell. Sentaurus Visual was used to analyze and visualize the results obtained on the Sentaurus Device, and Sentaurus Workbench tools were used to manage the simulation process and to work together with the instruments.

B. THEORETICAL BACKGROUND

In the simulation of solar cells, the first optical properties are determined. Sentaurus TCAD has 3 main methods for calculating optical properties: Transfer Matrix Method (TMM) [34], Ray Tracing [35] and Beam Propagation [36]. In the Ray Tracing method, a certain number of rays are put on the solar cell, and a separate calculation is made for each ray. At the border of two environments, the beam splits into reflected and refracted rays, each of which has its own set of calculations. Therefore, the Ray Tracing method is mainly used to model textured solar elements. One drawback of such method is its inability to calculate the transmission, reflection and absorption coefficients of solar cells depending on the wavelength of light. Its calculation accuracy depends on the number of rays. In TMM, according to Maxwell's electromagnetic field theory and Beer Lambert's law [37], matrices of electric field or magnetic field induction vectors are created, and the absorption, transmission and reflection coefficient of the whole system is calculated. TMM is the most suitable method for determining the optical properties of thin films as it takes into account the phenomenon of interference [38]. Since there is a possibility of Fano interference of light emitted from nanoparticles, in this research work, we also used TMM to model nanoparticle embedded solar cells. Regardless of the used methods, optical boundary conditions are typically divided into: angular and energy. The relationship between the angles of incidence, refraction and reflection of light incident on the boundary of two media is determined using Snell's law given in formula 1 [39], and this is considered an angle boundary condition. The relationship between the energies of incident, refracted and reflected rays is calculated using the Fresnel coefficients given in formula 2 [40].

$$\frac{n_1}{n_2} = \frac{\sin(\gamma)}{\sin(\theta)}, \quad \beta = \theta \quad (1)$$

Here: θ is the angle of the reflected light, n_1 and n_2 refractive indices of the media, γ is the angle of the refracted light.

$$\begin{cases} r_t = \frac{n_1 \cos \beta - n_2 \cos \gamma}{n_1 \cos \beta + n_2 \cos \gamma} \\ t_t = \frac{2n_1 \cos \beta}{n_1 \cos \beta + n_2 \cos \gamma} \\ r_p = \frac{n_1 \cos \gamma - n_2 \cos \beta}{n_1 \cos \gamma + n_2 \cos \beta} \\ t_p = \frac{2n_1 \cos \beta}{n_2 \cos \beta + n_1 \cos \gamma} \end{cases} \quad (2)$$

Here: r_t and t_t are the Fresnel coefficients for transversal polarized light, r_p and t_p are the Fresnel coefficients for parallel polarized light, β is the angle of incident light, γ is the angle of refracted light.

After determining the optical properties in TMM, the generation coefficient is calculated using the quantum yield function. The quantum yield is a logic function that takes 1 if the photon energy is greater than or equal to the material's bandgap, and 0 otherwise.

There are mainly 3 types of recombination in semiconductors [41]: Radiative, Shockley-Read-Hall (SRH) and Auger. Since silicon is an indirect semiconductor, it mainly has SRH and Auger recombination, Radiative recombination is almost absent. ZnO and perovskite are direct semiconductors, they have three types of recombination. Therefore, separate recombination models were used for each region in the modeling. For example, since the emitter region is made of ZnO or Perovskite, all three recombinations have been declared to exist, and since the base is made of silicon, only SRH and Auger recombinations have been declared to exist. SRH recombination due to defects is calculated using formula 3 [42].

$$R_{net}^{SRH} = \frac{np - \gamma_n \gamma_p n_i^2}{\tau_p (n + \gamma_n n_1) + \tau_n (p + \gamma_p p_1)} \quad (3)$$

Here: n is the electron concentration, p is the hole concentration, γ_n, γ_p are the coefficients, τ_n, τ_p are the electron and the hole lifetime, n_1, p_1 are the electron and the hole concentration on the trap.

Auger recombination is calculated using formula 4 [43] and is also called three particles recombination. Accordingly, as the concentration of charge carriers increases, so does its portion in the total recombination. An increase in the input concentration causes an increase in the concentration of charge carriers. Therefore, after the input concentration reaches a certain critical value, Auger recombination begins to dominate.

$$R_{net}^A = (C_n n + C_p p) (np - n_i^2) \quad (4)$$

Here: C_n, C_p are Auger coefficients. n_i is the intrinsic carrier concentration.

The electrostatic field formed around the charge carriers and ionized impurities and the electric potential are calculated using the Poisson equation in formula 5 [44].

$$\Delta \varphi = -\frac{q}{\varepsilon} (p - n - N_D + N_A) \quad (5)$$

Here: ε is the permittivity, N_D and N_A are the concentrations of donor and acceptor, q is the charge.

The internal electric field created by the ions in the p-n junction separates the electron-hole pairs and help to reach them to the contacts. So, unlike the diode, the drift movement of charge carriers plays the main role in the solar cell. The Masetti formula is given in formula 6 [45] was used to calculate the mobility of charge carriers. Because in the Masetti model, the effect of electron-phonon scattering, input concentration and temperature are also considered. Consequently, this model is suitable for estimating the mobility of charge carriers in nanoparticle-incorporated solar cells.

$$\begin{aligned} \mu_{dop} = & \mu_{min1} \exp\left(-\frac{P_c}{N_{A,0} + N_{D,0}}\right) \\ & + \frac{\mu_{const} + \mu_{min2}}{1 + ((N_{A,0} + N_{D,0})/c_r)^\alpha} \\ & - \frac{\mu_1}{1 + (C_s/(N_{A,0} + N_{D,0}))^\beta} \end{aligned} \quad (6)$$

Here: $\mu_{min}, \mu_{min2}, \mu_1$ are the constants related to the type of materials, P_c, C_r, C_s are the constants related to the doping concentration and material type, α, β are the fitting parameters, μ_{const} is the mobility depending on the temperature and the electron-phonon scattering, $N_{A,0}, N_{D,0}$ are the acceptor and donor concentration.

The free electrons inside a nanoparticle begin to vibrate as soon as the light hits its surface. If the vibration frequency of free electrons match that of the vibration frequency of the external electromagnetic field, a resonance phenomenon takes place giving the oscillating electron enough energy to escape the nanoparticle. Energy levels in metal are almost continuous, that is, the difference between two energy levels is smaller than thermal energy (kT). Quantum effects occur whenever the metal is shrunk to a very small scale "called critical size", at which point the gap between energy levels becomes greater than the thermal energy (kT). For example, the critical size for a gold nanoparticle is 100 nm [46]. Therefore, when light is applied, the electrons in the nanoparticle jump from one energy level to another, emitting phonons along the way. Due to the vibration of free electrons, an electromagnetic wave in the spectrum corresponding to the vibration frequency is radiated. Thus, Nanoparticles emit electrons, phonons, and high-energy photons when exposed to light. In Sentaurus TCAD, there are 4 different methods for calculating the charge carriers transport: Drift-Diffusion, Thermodynamic, Hydrodynamic and Monte Carlo. Among these models, only the thermodynamic model considers the effect of the change in the temperature of the crystal lattice on the charge carriers transport. The phonons generated in the nanoparticle increase the temperature of its surroundings and affect the thermodynamic balance in the solar cell. Therefore, in this scientific work, the thermodynamic model in formula 7 [47] was used to calculate the charge carriers transport in the nanoparticle introduced solar cell.

$$\begin{aligned} \vec{J}_n &= -nq\mu_n(\nabla\Phi_n + P_n\nabla T) \\ \vec{J}_p &= -pq\mu_p(\nabla\Phi_p + P_p\nabla T) \end{aligned} \quad (7)$$

Here: μ_n, μ_p are the mobilities of electron and holes, F_n, F_p are the electron and hole quasi-Fermi potentials, P_n, P_p are the thermoelectric power of electrons and holes, T is the absolute temperature.

In the thermodynamic model, the temperature of the crystal lattice must be taken into account; otherwise, the results obtained in this model will be the same as those obtained in the drift-diffusion model. To determine the temperature of the crystal lattice, the temperature differential equation in formula 8 [48] was used.

$$\begin{aligned} & \frac{\partial}{\partial t}(c_L T) - \nabla \cdot (k \nabla T) \\ &= -\nabla \cdot \left[(PT + \Phi_M) \vec{J}_M \right] \\ & - \frac{1}{q} \left(E_C + \frac{3}{2} kT \right) (\nabla \cdot \vec{J}_n - q R_{net,n}) \\ & - \frac{1}{q} \left(-E_V + \frac{3}{2} kT \right) (-\nabla \cdot \vec{J}_p - q R_{net,p}) + \hbar \omega G^{opt} \end{aligned} \quad (8)$$

Here: k is the heat conductance, c_L is the heat capacity, E_C is the minimum energy of conduction band, E_V is the maximum energy of valence band, G_{opt} is the optical generation, $R_{net,n}$ and $R_{net,p}$ are the net recombination, J_n and J_p are the current densities of electrons and holes, t is the time, F_m is the metal Fermi state, J_m is the current density in metal, ω is the frequency of photons, \hbar is the Planck constant.

The electric current and potential distribution at the nanoparticle/semiconductor and contact/semiconductor boundaries were determined using Ohmic boundary conditions in formula 9 [49]. Because there is an ohmic transition at the intersection of gold nanoparticle and semiconductor and metal contact and semiconductor according to their Fermi and conduction state energies.

$$\begin{aligned} \varphi &= \varphi_F + \frac{kT}{q} a \sinh \left(\frac{N_D - N_A}{2n_{i,eff}} \right) \\ n_0 p_0 &= n_{i,eff}^2 \\ n_0 &= \sqrt{\frac{(N_D - N_A)^2}{4} + n_{i,eff}^2} + \frac{N_D - N_A}{2} \\ p_0 &= \sqrt{\frac{(N_D - N_A)^2}{4} + n_{i,eff}^2} - \frac{N_D - N_A}{2} \end{aligned} \quad (9)$$

Here: $n_{i,eff}$ is the effective intrinsic carrier concentration, φ_F is the Fermi potential of contact.

III. RESULTS AND DISCUSSION

The main photoelectric parameters of solar cells are short circuit current, open circuit voltage, fill factor and output power. In Figure 1, the dependence of the short-circuit current of Perovskite/Si (a) and ZnO/Si (b) solar cells with gold nanoparticles with various size and periodicity is represented by a contour graph. The radius of the nanoparticle was changed from 4 nm to 20 nm, and the periodicity was changed from 60 nm to 200 nm. Depending on the periodicity of

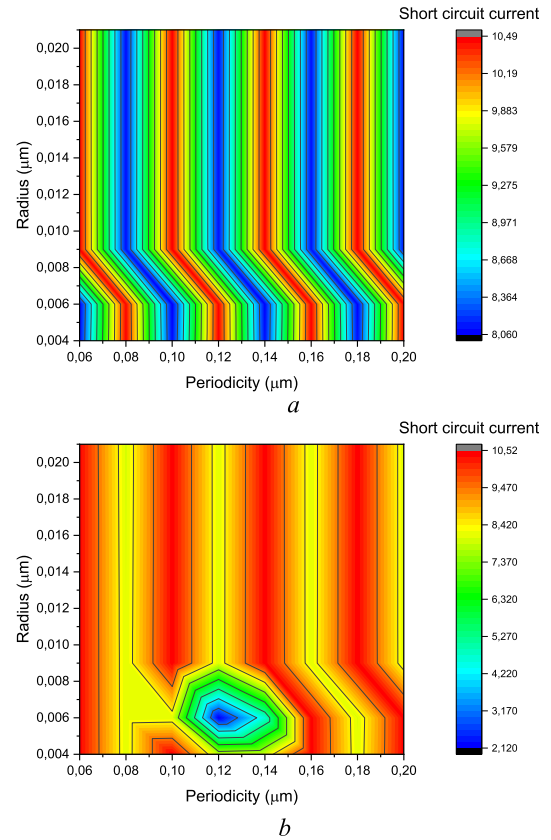


FIGURE 1. Short-circuit current of nanoparticle introduced to Perovskite/Si (a) and ZnO/Si (b) solar cells as a function of nanoparticle size and periodicity.

the nanoparticle, the short-circuit current of the perovskite/Si (Figure 1.a) solar cell varied periodically. According to the result in Figure 1.a, the radius dependence of the short-circuit current of the perovskite/Si solar cell can be divided into three ranges: (4 nm, 6 nm), (6 nm, 9 nm) and (9 nm, 21 nm). In the first and third ranges, the dependence of the short-circuit current on the periodicity of the nanoparticle did not show any variation, while it varied linearly in the range of (6 nm, 9 nm). On the other hand, the dependence of the short-circuit current of the ZnO/Si (Fig. 1.b) solar cell on the periodicity of nanoparticles has nothing to show in the ranges of the radius (9 nm, 21 nm). However, in the (4 nm, 9 nm) interval, the functional dependence of the short-circuit current on the periodicity of the nanoparticles disappeared, unlike the perovskite/Si solar cell.

It was found that there is a clear functional relationship in the dependence of the short-circuit current of the perovskite/Si solar cell on the periodicity of the nanoparticles. The functions were different between the third range (9 nm, 21 nm) and the first one (4 nm, 6 nm). Therefore, Fig. 2 shows the dependence of the short-circuit current of the perovskite/Si solar cell with a gold nanoparticle of 4 nm radius and 11 nm periodicity. From this graph, it became clear that the short-circuit current varies according to the periodic sinusoidal pattern depending on the distance between the nanoparticles. When the nanoparticle size changed from

4 nm to 11 nm, the maximum and minimum values of the short-circuit current did not change at all, only the phase of the sinusoidal connection changed to π phase. Electromagnetic waves emitted by nanoparticles can experience interference due to the phase difference with respect to the free electrons oscillations [50]. This interference is called Fano interference [51].

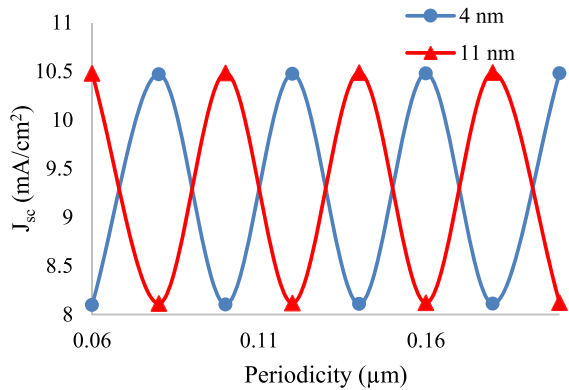


FIGURE 2. Dependence of the short-circuit current of Perovskite/Si solar cells containing gold nanoparticles with a radius of 4 nm and 11 nm on the nanoparticle periodicity.

Logical variable a was introduced into this formula. It was found that $\alpha = 0$ if the nanoparticle size is in the range (4 nm, 6 nm) and $\alpha = 1$ if it is in the range (9 nm, 21 nm). According to the results of simulation, it was determined that $J_{\max} = 10.47 \text{ mA/cm}^2$ and $J_{\min} = 8.11 \text{ mA/cm}^2$ for the perovskite/Si solar cell. However, the nanoparticle size had no effect on the maximum and minimum values of the short-circuit current of the perovskite/Si solar cell. This means that the amplitude of the Fano resonance is independent of the size of the nanoparticle unlike its phase. The short-circuit current $J = J_{\min}$ corresponds to Fano interference minimum state and $J = J_{\max}$ corresponds to the maximum state. That is, the short-circuit current of the perovskite/Si solar cell changes depending on the distance between the nanoparticles due to Fano interference. The short-circuit current of the perovskite/Si solar cell without nanoparticle was equal to the minimum short-circuit current of the perovskite/Si solar cell with gold nanoparticle. In order to scientifically justify the obtained results, Figure 3 shows the wavelength dependence of the absorption coefficient of the perovskite/Si solar cell with gold nanoparticle ($d_p = 80 \text{ nm}$, $r = 4 \text{ nm}$) and ($d_p = 80 \text{ nm}$, $r = 11 \text{ nm}$). Because ($d_p = 80 \text{ nm}$, $r = 4 \text{ nm}$) nanoparticle introduced solar cell achieved minimum and ($d_p = 80 \text{ nm}$, $r = 11 \text{ nm}$) maximum short circuit current. In the short wavelength's spectrum, the solar cell ($d_p = 80 \text{ nm}$, $r = 11 \text{ nm}$) has achieved a high absorption coefficient. In the visible spectrum, ($d_p = 80 \text{ nm}$, $r = 4 \text{ nm}$) the absorption of the solar cell was greater. The energy of short-wavelength photons is high, and the energy of the electron-holes formed due to their absorption is also high [52]. The probability of their recombination is high [53]. Therefore, the short circuit current of ($d_p = 80 \text{ nm}$, $r = 4 \text{ nm}$)

solar cell was higher than that of ($d_p = 80 \text{ nm}$, $r = 11 \text{ nm}$).

$$J = \frac{J_{\max} + J_{\min}}{2} + \frac{J_{\max} - J_{\min}}{2} \cos \left(\left(\frac{d_p}{2} + a \right) \pi \right),$$

$$\begin{cases} a = 0, & \text{if } r \in (4 \text{ nm}, 6 \text{ nm}) \\ a = 1, & \text{if } r \in (9 \text{ nm}, 21 \text{ nm}) \end{cases} \quad (10)$$

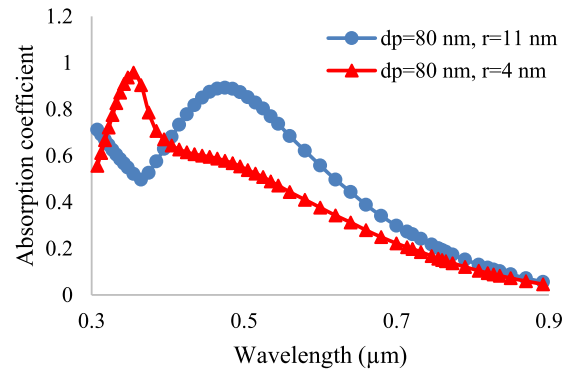


FIGURE 3. Dependence of the absorption coefficient of a perovskite/Si solar cell on wavelength.

According to the result presented by Figure 1.b, the short-circuit current of the ZnO/Si solar cell in the range of nanoparticle radius (9 nm, 21 nm) varies according to the exact law depending on the periodicity of nanoparticles. However, in the range of nanoparticle radius (4 nm, 9 nm) it was found that it does not obey the rules. Therefore, Figure 4 shows the dependence of the short-circuit current of a ZnO/Si solar cell with a nanoparticle with a radius of 6 nm and 11 nm on the nanoparticle periodicity. The short-circuit current of a ZnO/Si solar cell with a size of 11 nm nanoparticles varied periodically depending on the distance between the nanoparticles, like a perovskite/Si solar cell. There was an unusual shift in the short circuit current at 6 nm of nanoparticle size. With a separation of 120 nm between nanoparticles, the short circuit current drops to 2.13 mA/cm^2 . It was found that the short-circuit current of the ZnO/Si solar cell without nanoparticles was 8.11 mA/cm^2 . Hence, when gold nanoparticles with a size of 6 nm were introduced into a ZnO/Si solar cell with a periodicity of 120 nm, the short circuit current decreased by a factor of 3.81.

The minimum value of the short-circuit current of the ZnO/Si solar cell with a nanoparticle of 11 nm radius was equal to that of the ZnO/Si solar cell without the nanoparticle. The maximum value was 1.29 times greater than that of the ZnO/Si solar cell without the nanoparticle. In experiment [54], it was found that silver nanoparticles can boost efficiency of ZnO/Si heterojunction solar cell. In addition, the short-circuit current of the ZnO/Si solar cell can also be determined by formula 1. Figure 5 shows the dependence of the absorption coefficient of the ZnO/Si solar cell on the wavelength. The reason for the sharp decrease in the short circuit current of ZnO/Si solar cell with gold nanoparticle ($d_p = 120 \text{ nm}$, $r = 6 \text{ nm}$) is the sharp decrease in the absorption coefficient in the wavelength range of

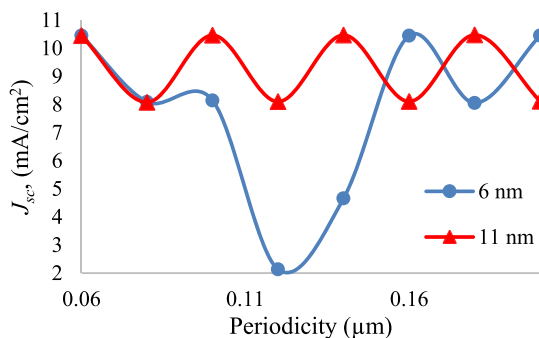


FIGURE 4. Dependence of the short-circuit current of the gold nanoparticles with radius of 6 nm and 11 nm introduced ZnO/Si solar cell on periodicity.

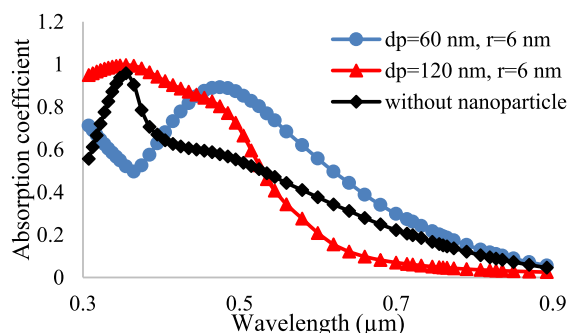


FIGURE 5. Dependence of the absorption coefficient of the ZnO/Si solar cell on the wavelength.

535-900 nm. Its absorption coefficient is almost reduced from that of the ZnO/Si solar cell without nanoparticle.

Figure 6 shows the dependence of the open circuit voltage and fill factor of perovskite/Si and ZnO/Si solar cells on nanoparticle size and periodicity. The open circuit voltage of perovskite/Si (Fig. 6.a) and ZnO/Si (Fig. 6.a') solar cells also changed depending on the nanoparticle size and periodicity, as did the short-circuit current. For the perovskite/Si solar cell, the maximum value of the open circuit voltage was 0.384 V, the minimum value was 0.366 V, and for the ZnO/Si solar cell, it was equal to 0.306 V and 0.27 V, respectively. The open circuit voltage of Perovskite/Si and ZnO/Si solar cells without nanoparticles is 0.3 V. Therefore, when a gold nanoparticle is introduced into a perovskite/Si solar cell, the efficiency increases significantly.

In the fill factor of perovskite/Si (Fig. 6.b), the sinusoidal relationship to the periodicity of the nanoparticle was preserved, only its phase changed to π . In the fill factor of ZnO/Si (Fig. 6.b'), a partial periodicity also occurred in the radius (4 nm, 9 nm) interval. The maximum value of the fill factor for perovskite/Si was 71.06%, the minimum value was 65.08%, and for ZnO/Si it was equal to 71.12% and 65.06%, respectively. The fill factor of perovskite/Si and ZnO/Si solar cells without nanoparticles is 70.28% and 70.6%, respectively. So, when the nanoparticle is introduced under optimal conditions, the fill factor almost increases.

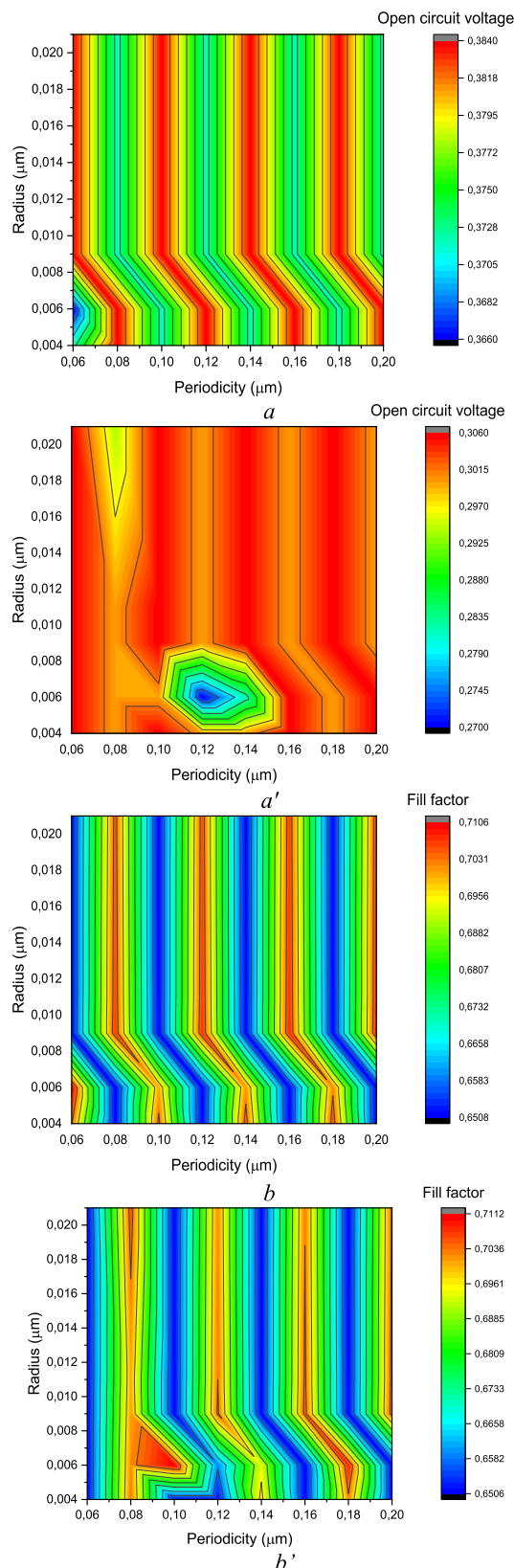


FIGURE 6. Dependence of the open circuit voltage (a, a') and fill factor (b, b') of perovskite/Si (a, b) and ZnO/Si (a', b') solar cells on nanoparticle size and periodicity.

IV. CONCLUSION

The formation of heterojunction on the surface of silicon increases the absorption coefficient of the silicon-based solar cell and improves the separation of charge carriers. In a ZnO/Si solar cell, ZnO acts as both an emitter and an anti-reflection layer. ZnO helps to absorb more photons in silicon. Since the absorption coefficient of perovskite is large in the perovskite/Si solar cell, it ensures more absorption of photons in the emitter layer as well. It was found that the introducing nanoparticles into the solar cell modify the light spectrum and cause the formation of additional electrons due to nanoplasmonic resonance and help to increase the absorption coefficient and short-circuit current of the solar cell. Therefore, in this scientific work, we introduced gold nanoparticles into the emitter layer of the solar cell. The dependence of photoelectric parameters of ZnO/Si and perovskite/Si solar cell on nanoparticle size and periodicity was studied. In conclusion, the short-circuit current of a perovskite/Si solar cell depends only on its periodicity, not on the size of the nanoparticle. The short-circuit current of the ZnO/Si solar cell is sinusoidal related to the periodicity of the nanoparticle but for perovskite/Si only in the nanoparticle size range (9 nm, 21 nm). It was found that the efficiency of perovskite/Si and ZnO/Si solar cells can be increased by a maximum of 1.25 times by introducing gold nanoparticles. Therefore, perovskite/Si and ZnO/Si heterojunctions with gold nanoparticles can be used in other optoelectronic devices and sensors. A Sol-Gel method for growing n-type perovskite and ZnO layers on p-type silicon was developed. Currently, we are looking for an experimental method of periodically inserting various metal nanoparticles into the emitter layer of the solar cell. Using the simulation results obtained here, we would like to experimentally create a silicon-based solar cell with a high efficiency in our next scientific work.

REFERENCES

- [1] C. Ballif, F.-J. Haug, M. Boccard, P. J. Verlinden, and G. Hahn, "Status and perspectives of crystalline silicon photovoltaics in research and industry," *Nature Rev. Mater.*, vol. 7, no. 8, pp. 597–616, Mar. 2022, doi: [10.1038/s41578-022-00423-2](https://doi.org/10.1038/s41578-022-00423-2).
- [2] M. Valiei, P. M. Shaibani, H. Abdizadeh, M. Kolahdouz, E. A. Soleimani, and J. Poursafar, "Design and optimization of single, double and multilayer anti-reflection coatings on planar and textured surface of silicon solar cells," *Mater. Today Commun.*, vol. 32, Aug. 2022, Art. no. 104144, doi: [10.1016/j.mtcomm.2022.104144](https://doi.org/10.1016/j.mtcomm.2022.104144).
- [3] J. Gulomov, R. Aliev, and B. Urmanov, "Effect of the thickness on photoelectric parameters of a textured silicon solar cell," *J. Surf. Invest., X-ray, Synchrotron Neutron Techn.*, vol. 16, no. 3, pp. 416–420, Jun. 2022, doi: [10.1134/S1027451022030375](https://doi.org/10.1134/S1027451022030375).
- [4] M. S. S. Basyoni, A. Zekry, and A. Shaker, "Investigation of base high doping impact on the NPN solar cell microstructure performance using physically based analytical model," *IEEE Access*, vol. 9, pp. 16958–16966, 2021, doi: [10.1109/ACCESS.2021.3053625](https://doi.org/10.1109/ACCESS.2021.3053625).
- [5] S. Kashyap, J. Madan, R. Pandey, and J. Ramanujam, "22.8% efficient ion implanted PERC solar cell with a roadmap to achieve 23.5% efficiency: A process and device simulation study," *Opt. Mater.*, vol. 128, Jun. 2022, Art. no. 112399, doi: [10.1016/j.optmat.2022.112399](https://doi.org/10.1016/j.optmat.2022.112399).
- [6] T. Markvart, "Shockley: Queisser detailed balance limit after 60 years," *WIREs Energy Environ.*, vol. 11, no. 4, p. e430, Jul. 2022, doi: [10.1002/WENE.430](https://doi.org/10.1002/WENE.430).
- [7] Y. Xu, T. Gong, and J. N. Munday, "The generalized Shockley-Queisser limit for nanostructured solar cells," *Sci. Rep.*, vol. 5, no. 1, pp. 1–9, Sep. 2015, doi: [10.1038/srep13536](https://doi.org/10.1038/srep13536).
- [8] J. Gulomov and R. Aliev, "The way of the increasing two times the efficiency of silicon solar cell," *Phys. Chem. Solid State*, vol. 22, no. 4, pp. 756–760, Dec. 2021, doi: [10.15330/PCSS.22.4.756-760](https://doi.org/10.15330/PCSS.22.4.756-760).
- [9] J. Schön, G. M. M. W. Bissels, P. Mulder, R. H. van Leest, N. Gruginskie, E. Vlieg, D. Chojniak, and D. Lackner, "Improvements in ultra-light and flexible epitaxial lift-off GaInP/GaAs/GaInAs solar cells for space applications," *Prog. Photovolt., Res. Appl.*, vol. 30, no. 8, pp. 1003–1011, Aug. 2022, doi: [10.1002/PIP.3542](https://doi.org/10.1002/PIP.3542).
- [10] D. Wang, Y. Wang, J. Huang, W. Fu, Y. Lei, P. Deng, H. Cai, and J. Liu, "Low-cost and flexible anti-reflection films constructed from nano multilayers of TiO₂ and SiO₂ for perovskite solar cells," *IEEE Access*, vol. 7, pp. 176394–176403, 2019, doi: [10.1109/ACCESS.2019.2957583](https://doi.org/10.1109/ACCESS.2019.2957583).
- [11] A. W. Faridi, M. Imran, G. H. Tariq, S. Ullah, S. F. Noor, S. Ansar, and F. Sher, "Synthesis and characterization of high-efficiency halide perovskite nanomaterials for light-absorbing applications," *Ind. Eng. Chem. Res.*, vol. 2022, pp. 1–15, Apr. 2022, doi: [10.1021/ACS.IECR.2C00416](https://doi.org/10.1021/ACS.IECR.2C00416).
- [12] N. Ali, N. Shehzad, S. Uddin, R. Ahmed, M. Jabeen, A. Kalam, A. G. Al-Sehemi, H. Alrobei, M. B. Kanoun, A. Khesro, and S. Goumri-Said, "A review on perovskite materials with solar cell prospective," *Int. J. Energy Res.*, vol. 45, no. 14, pp. 19729–19745, Nov. 2021, doi: [10.1002/ER.7067](https://doi.org/10.1002/ER.7067).
- [13] M. S. S. Basyoni, M. M. Salah, M. Mousa, A. Shaker, A. Zekry, M. Abouelatta, M. T. Alshammari, K. A. Al-Dhlan, and C. Gontrand, "On the investigation of interface defects of solar cells: Lead-based vs lead-free perovskite," *IEEE Access*, vol. 9, pp. 130221–130232, 2021, doi: [10.1109/ACCESS.2021.3114383](https://doi.org/10.1109/ACCESS.2021.3114383).
- [14] K. P. Ong, S. Wu, T. H. Nguyen, D. J. Singh, Z. Fan, M. B. Sullivan, and C. Dang, "Multi band gap electronic structure in CH₃NH₃PbI₃," *Sci. Rep.*, vol. 9, no. 1, pp. 1–8, Feb. 2019, doi: [10.1038/s41598-018-38023-2](https://doi.org/10.1038/s41598-018-38023-2).
- [15] S. A. Moiz, A. N. M. Alahmadi, and A. J. Aljohani, "Design of a novel lead-free perovskite solar cell for 17.83% efficiency," *IEEE Access*, vol. 9, pp. 54254–54263, 2021, doi: [10.1109/ACCESS.2021.3070112](https://doi.org/10.1109/ACCESS.2021.3070112).
- [16] J. Gulomov, O. Accouche, R. Aliev, B. Neji, R. Ghandour, I. Gulomova, and M. Azab, "Geometric optimization of perovskite solar cells with metal oxide charge transport layers," *Nanomaterials*, vol. 12, no. 15, p. 2692, Aug. 2022, doi: [10.3390/NANO12152692](https://doi.org/10.3390/NANO12152692).
- [17] Y. Chen, X. Zuo, Y. He, F. Qian, S. Zuo, Y. Zhang, L. Liang, Z. Chen, K. Zhao, Z. Liu, J. Gou, and S. Liu, "Dual passivation of perovskite and SnO₂ for high-efficiency MAPbI₃ perovskite solar cells," *Adv. Sci.*, vol. 8, no. 5, Mar. 2021, Art. no. 2001466, doi: [10.1002/ADVS.202001466](https://doi.org/10.1002/ADVS.202001466).
- [18] B. Ge, Z. Q. Lin, Z. R. Zhou, H. W. Qiao, A. P. Chen, Y. Hou, S. Yang, and H. G. Yang, "Boric acid mediated formation and doping of NiO_x layers for perovskite solar cells with efficiency over 21%," *Sol. RRL*, vol. 5, no. 4, Apr. 2021, Art. no. 2000810, doi: [10.1002/SOLR.202000810](https://doi.org/10.1002/SOLR.202000810).
- [19] V. M. Caselli and T. J. Savenije, "Quantifying charge carrier recombination losses in MAPbI₃/C60 and MAPbI₃/Spiro-OMeTAD with and without bias illumination," *J. Phys. Chem. Lett.*, vol. 2022, pp. 7523–7531, Aug. 2022, doi: [10.1021/ACS.JPCLETT.2C01728](https://doi.org/10.1021/ACS.JPCLETT.2C01728).
- [20] A. A. B. Baloch, M. I. Hossain, N. Tabet, and F. H. Alharbi, "Practical efficiency limit of methylammonium lead iodide perovskite (CH₃NH₃PbI₃) solar cells," *J. Phys. Chem. Lett.*, vol. 9, no. 2, pp. 426–434, Jan. 2018, doi: [10.1021/acs.jpclett.7b03343](https://doi.org/10.1021/acs.jpclett.7b03343).
- [21] W. E. I. Sha, X. Ren, L. Chen, and W. C. H. Choy, "The efficiency limit of CH₃NH₃PbI₃ perovskite solar cells," *Appl. Phys. Lett.*, vol. 106, no. 22, Jun. 2015, Art. no. 221104, doi: [10.1063/1.4922150](https://doi.org/10.1063/1.4922150).
- [22] R. Iacobellis, S. Masi, A. Rizzo, R. Grisorio, M. Ambrico, S. Colella, P. F. Ambrico, G. P. Suranna, A. Listorti, and L. De Marco, "Addressing the function of easily synthesized hole transporters in direct and inverted perovskite solar cells," *ACS Appl. Energy Mater.*, vol. 1, no. 3, pp. 1069–1076, Mar. 2018, doi: [10.1021/ACSAEM.7B00208](https://doi.org/10.1021/ACSAEM.7B00208).
- [23] F. K. Aldibaja, L. Badia, E. Mas-Farzá, R. S. Sánchez, E. M. Barea, and I. Mora-Sero, "Effect of different lead precursors on perovskite solar cell performance and stability," *J. Mater. Chem. A*, vol. 3, no. 17, pp. 9194–9200, 2015, doi: [10.1039/C4TA06198E](https://doi.org/10.1039/C4TA06198E).
- [24] G. Gokceli, S. Bozar, and N. Karatepe, "Optimization of inverted CH₃NH₃PbI₃ based perovskite solar cells by experimental design," *Int. J. Energy Res.*, vol. 46, no. 6, pp. 7655–7665, May 2022, doi: [10.1002/ER.7666](https://doi.org/10.1002/ER.7666).
- [25] J. Gulomov and R. Aliev, "Influence of the angle of incident light on the performance of textured silicon solar cells," *J. Nano-Electron. Phys.*, vol. 13, no. 6, pp. 06036-1–06036-5, 2021, doi: [10.21272/JNEP.13\(6\).06036](https://doi.org/10.21272/JNEP.13(6).06036).

- [26] Y. Jiang, "Efficient colorful perovskite solar cells using a top polymer electrode simultaneously as spectrally selective antireflection coating," *Nano Lett.*, vol. 16, no. 12, pp. 7829–7835, Dec. 2016, doi: [10.1021/ACS.NANOLETT.6B04019](https://doi.org/10.1021/ACS.NANOLETT.6B04019).
- [27] L. Yue, B. Yan, M. Attridge, and Z. Wang, "Light absorption in perovskite solar cell: Fundamentals and plasmonic enhancement of infrared band absorption," *Sol. Energy*, vol. 124, pp. 143–152, Feb. 2016, doi: [10.1016/J.SOLENER.2015.11.028](https://doi.org/10.1016/J.SOLENER.2015.11.028).
- [28] A. I. Anghi, M. R. Islam, M. T. Hasan, and E. Hossain, "Projected performance of InGaAs/GaAs quantum dot solar cells: Effects of cap and passivation layers," *IEEE Access*, vol. 8, pp. 212339–212350, 2020, doi: [10.1109/ACCESS.2020.3039457](https://doi.org/10.1109/ACCESS.2020.3039457).
- [29] N. L. Chang, J. Zheng, Y. Wu, H. Shen, F. Qi, K. Catchpole, A. Ho-Baillie, and R. J. Egan, "A bottom-up cost analysis of silicon-perovskite tandem photovoltaics," *Prog. Photovolt., Res. Appl.*, vol. 29, no. 3, pp. 401–413, Mar. 2021, doi: [10.1002/PIP.3354](https://doi.org/10.1002/PIP.3354).
- [30] L. Q. Cao, Z. He, W. E. I. Sha, and R.-S. Chen, "Influence of geometry of metallic nanoparticles on absorption of thin-film organic solar cells: A critical examination," *IEEE Access*, vol. 8, pp. 145950–145959, 2020, doi: [10.1109/ACCESS.2020.3014817](https://doi.org/10.1109/ACCESS.2020.3014817).
- [31] J. Gulomov, O. Accouche, R. Aliev, M. Azab, and I. Gulomova, "Analyzing the ZnO and CH₃NH₃PbI₃ as emitter layer for silicon based heterojunction solar cells," *Comput., Mater. Continua*, vol. 74, no. 1, pp. 575–590, 2023, doi: [10.32604/CMC.2023.031289](https://doi.org/10.32604/CMC.2023.031289).
- [32] J. Zhao, Z. Xu, M.-K. Law, H. Heidari, S. O. Abdellatif, M. A. Imran, and R. Ghannam, "Simulation of crystalline silicon photovoltaic cells for wearable applications," *IEEE Access*, vol. 9, pp. 20868–20877, 2021, doi: [10.1109/ACCESS.2021.3050431](https://doi.org/10.1109/ACCESS.2021.3050431).
- [33] M. K. Abduvohidov, R. Aliev, and J. Gulomov, "A study of the influence of the base thickness on photoelectric parameters of silicon solar cells with the new TCAD algorithms," *Sci. Tech. J. Inf. Technol., Mech. Opt.*, vol. 21, no. 5, pp. 774–784, Oct. 2021, doi: [10.17586/2226-1494-2021-21-5-774-784](https://doi.org/10.17586/2226-1494-2021-21-5-774-784).
- [34] M. Zinser, T. Helder, A. Bauer, T. M. Friedlmeier, J. Zillner, J.-P. Becker, and M. Powalla, "Optical and electrical loss analysis of thin-film solar cells combining the methods of transfer matrix and finite elements," *IEEE J. Photovolt.*, vol. 12, no. 5, pp. 1154–1161, Sep. 2022, doi: [10.1109/JPHOTOV.2022.3190770](https://doi.org/10.1109/JPHOTOV.2022.3190770).
- [35] N. Wöhrle, J. Greulich, C. Schwab, M. Glatthaar, and S. Rein, "A predictive optical simulation model for the rear-surface roughness of passivated silicon solar cells," *IEEE J. Photovolt.*, vol. 3, no. 1, pp. 175–182, Jan. 2013, doi: [10.1109/JPHOTOV.2012.2215013](https://doi.org/10.1109/JPHOTOV.2012.2215013).
- [36] D. Schulz, C. Glingener, M. Bludszuweitz, and E. Voges, "Mixed finite element beam propagation method," *J. Lightw. Technol.*, vol. 16, no. 7, pp. 1336–1341, Jul. 15, 1998, doi: [10.1109/50.701414](https://doi.org/10.1109/50.701414).
- [37] U. Asgher, R. Ahmad, N. Naseer, Y. Ayaz, M. J. Khan, and M. K. Amjad, "Assessment and classification of mental workload in the prefrontal cortex (PFC) using fixed-value modified Beer-Lambert law," *IEEE Access*, vol. 7, pp. 143250–143262, 2019, doi: [10.1109/ACCESS.2019.2944965](https://doi.org/10.1109/ACCESS.2019.2944965).
- [38] C. C. Katsidis and D. I. Siapkas, "General transfer-matrix method for optical multilayer systems with coherent, partially coherent, and incoherent interference," *Appl. Opt.*, vol. 41, no. 19, pp. 3978–3987, Jul. 2002, doi: [10.1364/AO.41.003978](https://doi.org/10.1364/AO.41.003978).
- [39] O. Litzman and P. Rózsa, "The interaction of light with a semiinfinite dielectric as a phonon problem; the generalized Snellius law and Fresnel formulae," *Surf. Sci.*, vol. 66, no. 2, pp. 542–558, Sep. 1977, doi: [10.1016/0039-6028\(77\)90037-1](https://doi.org/10.1016/0039-6028(77)90037-1).
- [40] Y. Xie, M. Sengupta, A. Habte, and A. Andreas, "The 'Fresnel equations' for diffuse radiation on inclined photovoltaic surfaces (FEDIS)," *Renew. Sustain. Energy Rev.*, vol. 161, Jun. 2022, Art. no. 112362, doi: [10.1016/J.RSER.2022.112362](https://doi.org/10.1016/J.RSER.2022.112362).
- [41] L. Höglund, D. Z. Ting, A. Khoshakhlagh, A. Soibel, C. J. Hill, A. Fisher, S. Keo, and S. D. Gunapala, "Influence of radiative and non-radiative recombination on the minority carrier lifetime in midwave infrared InAs/InAsSb superlattices," *Appl. Phys. Lett.*, vol. 103, no. 22, Nov. 2013, Art. no. 221908, doi: [10.1063/1.4835055](https://doi.org/10.1063/1.4835055).
- [42] D. Macdonald and A. Cuevas, "Validity of simplified Shockley-Read-Hall statistics for modeling carrier lifetimes in crystalline silicon," *Phys. Rev. B, Condens. Matter*, vol. 67, no. 7, Feb. 2003, Art. no. 075203, doi: [10.1103/PhysRevB.67.075203](https://doi.org/10.1103/PhysRevB.67.075203).
- [43] M. J. Kerr and A. Cuevas, "General parameterization of Auger recombination in crystalline silicon," *J. Appl. Phys.*, vol. 91, no. 4, p. 2473, Jan. 2002, doi: [10.1063/1.1432476](https://doi.org/10.1063/1.1432476).
- [44] I. D. Mayergoyz, "Solution of the nonlinear Poisson equation of semiconductor device theory," *J. Appl. Phys.*, vol. 59, no. 1, p. 195, Jun. 1998, doi: [10.1063/1.336862](https://doi.org/10.1063/1.336862).
- [45] S. Reggiani, M. Valdinoci, L. Colalongo, M. Rudan, G. Baccarani, A. D. Stricker, F. Illien, N. Felber, W. Fichtner, and L. Zullino, "Electron and hole mobility in silicon at large operating temperatures. I. Bulk mobility," *IEEE Trans. Electron Devices*, vol. 49, no. 3, pp. 490–499, Mar. 2002, doi: [10.1109/16.987121](https://doi.org/10.1109/16.987121).
- [46] D. L. García-Ruiz, F. G. Granados-Martínez, C. J. Gutiérrez-García, J. M. Ambríz-Torres, J. de Jesús Contreras-Navarrete, N. Flores-Ramírez, F. Méndez, and L. Domratcheva-Lvov, "Synthesis of carbon nanomaterials by chemical vapor deposition method using green chemistry principles," in *Handbook of Greener Synthesis of Nanomaterials and Compounds*. Amsterdam, The Netherlands: Elsevier, 2021, doi: [10.1016/B978-0-12-821938-6.00008-6](https://doi.org/10.1016/B978-0-12-821938-6.00008-6).
- [47] J. E. Parrott, "Thermodynamic theory of transport processes in semiconductors," *IEEE Trans. Electron Devices*, vol. 43, no. 5, pp. 809–826, May 1996, doi: [10.1109/16.491259](https://doi.org/10.1109/16.491259).
- [48] G. K. Wachutka, "Rigorous thermodynamic treatment of heat generation and conduction in semiconductor device modeling," *IEEE Trans. Comput.-Aided Design Integr. Circuits Syst.*, vol. 9, no. 11, pp. 1141–1149, Nov. 1990, doi: [10.1109/43.62751](https://doi.org/10.1109/43.62751).
- [49] M. G. Ancona, D. Yergeau, Z. Yu, and B. A. Biegel, "On ohmic boundary conditions for density-gradient theory," *J. Comput. Electron.*, vol. 1, no. 1/2, pp. 103–107, 2002, doi: [10.1023/A:1020728130470](https://doi.org/10.1023/A:1020728130470).
- [50] F. Ramirez, P. R. Heyliger, A. K. Rappé, and R. G. Leisure, "Vibrational modes of free nanoparticles: From atomic to continuum scales," *J. Acoust. Soc. Amer.*, vol. 123, no. 2, p. 709, Feb. 2008, doi: [10.1121/1.2823065](https://doi.org/10.1121/1.2823065).
- [51] A. M. Fales, S. J. Norton, B. M. Crawford, B. G. DeLacy, and T. Vo-Dinh, "Fano resonance in a gold nanosphere with a J-aggregate coating," *Phys. Chem. Chem. Phys.*, vol. 17, no. 38, pp. 24931–24936, 2015, doi: [10.1039/C5CP03277F](https://doi.org/10.1039/C5CP03277F).
- [52] Z. C. Holman, A. Descoeudres, L. Barraud, F. Z. Fernandez, J. P. Seif, S. De Wolf, and C. Ballif, "Current losses at the front of silicon heterojunction solar cells," *IEEE J. Photovolt.*, vol. 2, no. 1, pp. 7–15, Jan. 2012, doi: [10.1109/JPHOTOV.2011.2174967](https://doi.org/10.1109/JPHOTOV.2011.2174967).
- [53] D. Madsen, C. L. Thomsen, J. Thøgersen, and S. R. Keiding, "Temperature dependent relaxation and recombination dynamics of the hydrated electron," *J. Chem. Phys.*, vol. 113, no. 3, p. 1126, Jul. 2000, doi: [10.1063/1.481891](https://doi.org/10.1063/1.481891).
- [54] P. Shokeen, A. Jain, and A. Kapoor, "Plasmonic ZnO/p-silicon heterojunction solar cell," *Opt. Mater.*, vol. 67, pp. 32–37, May 2017, doi: [10.1016/J.OPTMAT.2017.03.033](https://doi.org/10.1016/J.OPTMAT.2017.03.033).



JASURBEK GULOMOV was born in Andijan, Uzbekistan, in 1999. He received the B.S. degree in physics from Andijan State University, Uzbekistan, in 2021, where he is currently pursuing the master's degree in physics focusing on renewable energy sources and environmental sustainability. He is a Researcher with the Renewable Energy Sources Laboratory, Andijan State University. He is the author of 16 articles and seven inventions. His research interests include

numerical simulation, nanoplasmonic solar cells, metal nanoparticles, metal oxides, heterojunction solar cells, computational material science, and programming. He received the National Scholarship after being named Mirzo Ulugbek and is the winner of Student of the Year in 2021.



OUSSAMA ACCOUCHE (Associate Member, IEEE) received the degree in electrical engineering from the Lebanese University, Beirut, Lebanon, in 2011 and the master's and Ph.D. degrees in smart grids from Grenoble-Alpes University, Grenoble, France, in 2016. He has several years of industrial and international experience, including France, Italy, and Japan as a Supervisor Engineer. Since September 2018, he has been working as an Assistant Professor with the Electrical Engineering Department, American University of the Middle East, Egaila, Kuwait. His research interests include smart grids, renewable energies, solar cells, artificial intelligence, and smart cities.

...